DMD Fast Forward. Published on May 20, 2016 as DOI: 10.1124/dmd.115.068619
This article has not been copyedited and formatted. The final version may differ from this version.

DMD # 68619

Establishment of in silico prediction models for CYP3A4 and CYP2B6 induction in human hepatocytes by multiple regression analysis using azole compounds

Mika Nagai, Yoshihiro Konno, Masahiro Satsukawa, Shinji Yamashita, and Kouichi Yoshinari

Pharmacokinetics and Safety Department, Drug Research Center, Kaken Pharmaceutical Co., Ltd., Kyoto, Japan (M.N., Y.K., M.S.); Department of Molecular Toxicology, School of Pharmaceutical Sciences, University of Shizuoka, Shizuoka, Japan (M.N., K.Y.); and Faculty of Pharmaceutical Sciences, Setsunan University, Osaka, Japan (S.Y.)

DMD Fast Forward. Published on May 20, 2016 as DOI: 10.1124/dmd.115.068619
This article has not been copyedited and formatted. The final version may differ from this version.

DMD # 68619

Running title: In silico prediction models for CYP3A4 and CYP2B6 induction

All correspondence to: Mika Nagai

Pharmacokinetics and Safety Department,

Drug Research Center, Kaken Pharmaceutical Co., Ltd.

14, Shinomiya Minamigawara-cho,

Yamashina-ku, Kyoto, 607-8042, Japan

Telephone: 81-75-594-0787, Facsimile: 81-75-594-0790

E-mail: nagai_mika@kaken.co.jp

Number of text page:	33
Number of tables:	5
Number of figures:	6
Number of references:	37
Number of words in Abstract:	248
Number of words in Introduction:	702
Number of words in Discussion:	1329

Abbreviations: AHR, aryl hydrocarbon receptor; CAR, constitutive androstane receptor; CITCO, 6-(4-clorophenyl) imidazo[2,1-*b*][1,3]thiazole-5-carbaldehyde *O*-(3,4-dichlorobenzyl)oxime; CYP, cytochrome P450; DDI, drug-drug interaction; 3-MC, 3-methylcholanthrene; PCA, principal component analysis; PXR, pregnane X receptor

Abstract

Drug-drug interactions (DDIs) via CYP induction are one clinical problem leading to increased risk of adverse effects and the need for dosage adjustments and additional therapeutic monitoring. In silico models for predicting CYP induction is useful for avoiding DDI risk. In this study we have established regression models for CYP3A4 and CYP2B6 induction in human hepatocytes using several physicochemical parameters for a set of azole compounds with different CYP induction as characteristics as model compounds. To obtain a well-correlated regression model, the compounds for CYP3A4 or CYP2B6 induction were independently selected from the tested azole compounds using principal component analysis with fold-induction data. Both of the multiple linear regression models obtained for CYP3A4 and CYP2B6 induction are represented by different sets of physicochemical parameters. The adjusted coefficients of determination for these models were of 0.8 and 0.9, respectively. The fold-inductions of the validation compounds, another set of 12 azole-containing compounds, were predicted within 2-fold limits for both CYP3A4 and CYP2B6. The concordance for the prediction of CYP3A4 induction was 87% with another validation set, 23 marketed drugs. However, the prediction of CYP2B8 induction tended to be over-estimated for these marketed drugs. The regression models show that lipophilicity mostly contributes to CYP3A4 induction while not only the lipophilicity but also the molecular polarity is important for CYP2B6 induction. Our regression models, especially that for CYP3A4 induction might provide useful methods to avoid potent CYP3A4 or CYP2B6 inducers during the lead optimization stage without performing induction assays in human hepatocytes.

Introduction:

Drug-drug interactions (DDIs) can affect the pharmacokinetics of a co-administered drug or its metabolites, which consequently increases the risk of adverse effects from the drug and causes the need for dosage adjustment and additional therapeutic monitoring. Therefore, it is important to predict DDIs during the drug discovery process. In the past several years, the pharmaceutical regulatory agencies in the United States, Europe, and Japan have issued guideline/draft guidance documents for in vitro and in vivo DDI studies that need be conducted during the development of new drug candidates (http://www.fda.gov/downloads/Drugs/GuidanceComplianceRegulatoryInformation/Guidances/UCM292362.pdf, http://www.ema.europa.eu/docs/en_GB/document_library/Scientific_guideline/2012/07/WC500129606.pdf, http://www.nihs.go.jp/mhlw/20131488.pdf). To reduce DDI risks, several screening methods are conducted to design safer and more effective drug molecules.

The inhibition and/or induction of cytochrome P450s (CYPs) are the main mechanisms of DDIs. Several clinically used drugs cause CYP induction, including the antibiotic rifampicin (Niemi et al., 2003), the acyl-CoA/cholesterol acyltransferase inhibitor avasimibe (Sahi et al., 2003), and the dual endothelin receptor antagonist bosentan (Dingemanse and van Giersbergen, 2004). These drugs reduce the plasma concentration of midazolam and/or those of themselves. General induction mechanisms involve the activation of nuclear receptor-type transcription factors. Inducers directly bind to or indirectly activate one or more of the following receptors: aryl hydrocarbon receptor (AHR), pregnane X receptor (PXR), and constitutive androstane receptor (CAR). Among them, PXR plays a key role in the drug-mediated induction of CYP3A4, a major human drug metabolizing CYP (LeCluyse, 2001). Therefore, PXR activation is a good prediction marker for CYP3A4 induction (Luo et al., 2002). However, many of the ligands that activate PXR can also activate CAR and there is

DMD Fast Forward. Published on May 20, 2016 as DOI: 10.1124/dmd.115.068619
This article has not been copyedited and formatted. The final version may differ from this version.

an overlap in the target genes of these two receptors (Maglich et al., 2002, Maglich et al., 2003, Wei et al., 2002) and there are uncertainties about CYP3A4 induction with CAR activators and/or PXR/CAR dual agonists because there is no perfect reporter assay system of CAR (Imai, et al. 2013).

Although several prediction systems have been developed for the substrates and inhibitors of CYP enzymes (Mishra et al., 2010, and Wanchana et al., 2003), systems for CYP induction are limited. As an in silico approach to predict enzyme induction, computational ligand docking, QSAR approach using machine-learning methods, and classifications using recursive partitioning methods have been developed for PXR that plays a key role in CYP induction (Xiao et al., 2011, Wu et al., 2013, Khandelwal et al., 2008, Dybdahi et al., 2012, and Handa et al., 2015). Docking studies provide important interactions between ligands and proteins but have limitations in quantitative predictions. Although general QSAR models can provide a quantitative prediction, they require a large number of agonists to establish a reliable model. Therefore, a quantitative prediction model conducted with a moderate number of compounds and commonly used physicochemical parameters would be a useful tool in lead-optimizing and developing processes.

Conazoles are a class of *N*-substituted azole antifungal drugs, which include two major classes, namely, imidazole- and triazole-containing compounds. These azole-containing antifungals are also used as environmental agents to control fungal growth. Many conazoles inhibit ergosterol synthesis through the inhibition of fungal CYP51 (lanosterol 14α-demethylase) activity. Furthermore, these conazoles inhibit mammalian hepatic CYPs in the clinic (Niwa et al., 2014), especially because imidazole antimycotics are known to show extremely high affinity for the heme iron atom of CYP. In addition, a number of azole-containing compounds, including cyproconazole, fenbuconazole, propiconazole, fluconazole, triadimefon, and myclobutanil, have been reported with abilities to induce

CYP1A, CYP2B, CYP2C, and CYP3A enzymes in mouse livers (Juberg et al., 2006, Goetz et al., 2006, Sun et al., 2006, Sun et al., 2007). Voriconazole, a triazole-containing conazole, shows PXR- and CAR-mediated auto-induction in mice (Ohbuchi et al., 2013). Clotrimazole, also known as a CYP3A4 inducer, and its analogs were potent ligands of human PXR (Luo et al., 2002, Sahi et al., 2009, Matsuura et al., 1991). Therefore, the azole-containing compounds might be good model compounds for a CYP induction prediction model due to their variable abilities to induce CYPs.

In this study, we used a group of azole compounds for a learning set and established regression models with several physicochemical parameters for CYP3A4 and CYP2B6 induction in human hepatocytes. The accuracy and limitations of the models were clarified using another set of azole compounds and non-azole compounds (commercially used pharmaceutical drugs).

Materials and Methods

Materials. Climbazole, hexaconazole, triflumizole, and uniconazole were purchased from abcam Biochemicals (Tokyo, Japan). Fenbuconazole, imazalil, and lanoconazole were obtained from Santa Cruz Biotechnology (Santa Cruz, CA), AK Scientific (Union City, CA), and Sequoia Research Products (Pangbourne, UK), respectively. Bifonazole, clotrimazole, econazole, miconazole, avasimibe, flumazenil, nifedipine, rifampicin, 3-methylcholanthrene (3-MC), and 6-(4-clorophenyl)imidazo[2,1-*b*][1,3]thiazole-5-carbaldehyde *O*-(3,4-dichlorobenzyl)oxime (CITCO) were from Sigma-Aldrich (St. Louis, MO). Fluconazole, isoconazole, voriconazole, ethinyl estradiol, fluoxetine, ranitidine, and topiramate were purchased from Tokyo Chemical Industry (Tokyo, Japan). Myclobutanil, oxiconazole, propiconazole, tebuconazole, tioconazole, carbamazepine, gatifloxacin, leflunomide, nafcillin, phenobarbital, phenytoin, pioglitazone, and a metabolite of miconazole (1-(2,4-dichlorophenyl)-2-(1*H*-imidazol-1-yl)ethanol) were obtained from Wako Pure Chemical Industries (Osaka, Japan). Luliconazole, a metabolite of voriconazole (1-(2,4-difluorophenyl)-2-(1*H*-1,2,4-triazole-1-yl)ethanol), and the validation compounds containing imidazole moieties (WO 2008/156092) were produced at Kaken Pharmaceutical (Kyoto, Japan). Aprepitant, bosentan, efavirenz, fluvoxamine, pleconaril, probenecid, and troglitazone were from Axon Medchem (Reston, VA), Pharmten Chemical (Leshan, China), Tronto Research Chemicals (Tronto, Ontario, Canada), Tocris Bioscience (Bristol, UK), Cheminstock (Shanghai, China), Nacalai tesque (Kyoto, Japan), and Cayman Chemical (Ann Arbor, MI), respectively. Nevirapine and rosiglitazone were obtained from Chem Pacific (Zhejiang, China). Cryopreserved human hepatocytes, hepatocyte thawing, plating, and incubation media, antibiotics and Geltrex were purchased from Life Technologies (Carlsbad, CA). All other chemicals and reagents were of regent grade or better and were obtained from commercial sources.

DMD Fast Forward. Published on May 20, 2016 as DOI: 10.1124/dmd.115.068619
This article has not been copyedited and formatted. The final version may differ from this version.

Induction experiments using cryopreserved human hepatocytes. Cryopreserved human hepatocytes (lot no. Hu1423, Caucasian, male, 61 years old, and Hu8125, Caucasian, male, 44 years old) were thawed with thawing medium according to the manufacturer's protocol. The cells were seeded in collagen I pre-coated 96-well plates (Life Technologies) at a density of 0.5×10^5 viable cells/well. Viability was determined by trypan blue exclusion of 90% or better for this study. Cells were maintained in fetal bovine serum (Life Technologies)-added Williams' E medium (Life Technologies) at 37°C in a humidified incubator with an atmosphere of 5% CO_2-95% air for 4 to 6 h. Subsequently, the medium was changed to serum-free Williams' E medium (incubation medium) containing 0.35 mg/mL Geltrex. The following day, the medium was changed to fresh incubation medium, and the hepatocytes were incubated at 37°C. The medium was removed 24 h after plating, and the hepatocytes were treated with medium containing the test compounds for 48 h. Fresh medium containing the test compounds was supplied daily. The test compounds were used at a single concentration of 10 μM and the reference compounds, 3-MC (1 μM) for CYP1A2, phenobarbital (750 μM) and CITCO (1 μM) for CYP2B6, and rifampicin (10 μM) for CYP3A4, and probenecid (10 μM) as a negative control, were used to confirm the performance of hepatocyte preparations. Both test compounds and reference inducers were dissolved in dimethyl sulfoxide and the final concentration of dimethyl sulfoxide in the incubation medium was 0.1%.

mRNA level determination. A QuantiGene Plex 2.0 Assay Kit (Panel #12117) from Affymetrix (Santa Clara, CA) was used to determine mRNA levels. After a 48-h incubation period, the hepatocytes were washed with Krebs-Henseleit buffer and then lysed. The mRNA level determination was performed according to the manufacturer's protocol. *CYP1A2*,

DMD Fast Forward. Published on May 20, 2016 as DOI: 10.1124/dmd.115.068619
This article has not been copyedited and formatted. The final version may differ from this version.

CYP2B6, *CYP2C9*, and *CYP3A4* mRNA levels were normalized against the geometric mean value of two house-keeping genes; *PGK1* and *HPRT1*.

Data processing and model development. The optimized 3D conformations of the test compounds were generated using ChemBio3D Ultra 12.0 (PerkinElmer, Waltham, MA) and their physicochemical parameters were calculated with QikProp (Schrödinger, Mannheim, Germany) and clogP values were calculated with ChemBioDraw Ultra 12.0 (PerkinElmer). Regression models for CYP induction were established using the set of compounds shown in Fig. 1. Multiple linear regression modeling was performed using JMP 7 (SAS Institute Japan, Tokyo, Japan) with physicochemical parameters. The goodness of fit for the models was assessed using the adjusted coefficient of determination (R^2) and the root mean square error (RMSE):

$$\mathrm{RMSE} = \sqrt{\frac{\sum(\text{predicted fold-induction} - \text{observed fold-induction})^2}{\text{number of predictions}}}$$

The selection of variables was carried out by a stepwise forward-backward selection. To narrow the test compounds down based on their CYP induction profiles, principal component analysis (PCA) was performed using JMP 7 with fold-induction values of CYP1A2, CYP2B6, CYP2C9, CYP3A4 and a ratio of CYP3A4/CYP2B6.

Prediction of CYP3A4 and CYP2B6 induction using the regression models. Two types of validation compound sets were used to assess the predictive applicability; another set of azole compounds and a set of non-azole compounds (commercially marketed drugs used in the report by Fahmi et al.(2010)). For CYP3A4 induction of the marketed drugs, the predictive capability of the regression models established with the test compounds was assessed with the classification system including sensitivity, specificity, and concordance, which were defined

DMD Fast Forward. Published on May 20, 2016 as DOI: 10.1124/dmd.115.068619
This article has not been copyedited and formatted. The final version may differ from this version.

as follows:

$$\text{Sensitivity} = \frac{\text{Number of true positives}}{\text{Number of true positives} + \text{Number of false negatives}}$$

$$\text{Specificity} = \frac{\text{Number of true negatives}}{\text{Number of true negatives} + \text{Number of false positives}}$$

$$\text{Concordance} = \frac{\text{Number of true positives} + \text{Number of true negatives}}{\text{Total}}$$

To assess the applicability of the models for CYP3A4 and CYP2B6 induction using the different lots of hepatocytes, the fold-induction values of the test azole compounds in lot Hu8125 were predicted with the regression models established by lot Hu1423. Since the fold-induction values of non-inducers are always around 1 in any lots hepatocytes and the fold-induction values of inducers are usually different based on the characteristics of hepatocyte lots used, the potency of CYP induction was normalized using the fold-induction values of positive controls: rifampicin for CYP3A4 and CITCO for CYP2B6. The normalization was conducted using the following equation:

$y = A \times x + B$

x, y, A and B were the normalized predicted fold-induction value in lot Hu8125, the predicted fold-induction value in lot Hu1423, the slope and the intercept of the straight line used for the normalization.

The equation contained two points, (x, y) = (1, 1) and (an observed fold-induction value of positive control in lot Hu1423, an observed fold-induction value of positive control in lot Hu8125).

Results

CYP inductions in human hepatocytes.

Most of the imidazole- or triazole-containing compounds (Fig. 1) increased the mRNA levels of *CYP3A4* and *CYP2B6*, whereas only a few compounds, such as bifonazole and oxiconazole, increased the levels of *CYP1A2* more strongly than *CYP3A4* and *CYP2B6* (Table 1). The results indicated that climbazole etc. increased *CYP3A4* mRNA levels more than *CYP2B6* mRNA levels as rifampicin and that lanoconazole etc. increased *CYP2B6* mRNA levels more than *CYP3A4* mRNA levels as CITCO. 3-MC showed high selectivity to *CYP1A2* and probenecid, which was used as a negative control, increased the *CYP1A2*, *CYP2B6*, *CYP2C9*, and *CYP3A4* mRNA levels by less than 2-fold (Table 1).

Regression models for CYP3A4 and CYP2B6 induction.

The physicochemical parameters of the test compounds calculated are shown in Table 2 and Supplemental Table 1. The CYP3A4 and CYP2B6 fold-induction values showed no significant correlation with clogP or molecular weight (M.W.), which are commonly used molecular descriptors (Supplemental Figure 1). Therefore, the regression models using all of the test azole compounds did not predict the CYP3A4 and CYP2B6 induction with enough accuracy (R^2 = 0.4984 and RMSE = 2.7528 for CYP3A4 and R^2 = 0.6098 and RMSE = 1.7092 for CYP2B6) (Supplemental Figure 2).

To improve the regression models, we narrowed the list of test compounds using PCA with induction data. The loading plots and score plots are shown in Fig. 2. In the score plots, the preferential CYP3A4 inducers were plotted in the shadow area of PC1 vs. PC2 (Fig. 2C) and CYP2B6 inducers were plotted in the shadow area of PC1 vs. PC3 (Fig. 2 D). Therefore, these compounds in the shadow areas were selected and subjected to multiple linear regression modeling for each CYP3A4 and CYP2B6 induction. The physicochemical

parameters used in the regression model were selected by stepwise forward-backward methods within the criteria of p-values less than 0.05. The obtained regression models for CYP3A4 and CYP2B6 are as follows:

Fold-induction of CYP3A4 = 0.01799 × PISA + 1.7982 × clogP – 3.0211

Fold-induction of CYP2B6 = − 0.04472 × WPSA + 6.2242 × EA

− 0.03501 × SA fluorine + 1.9163 × clogP + 1.9622

With these regression models, fold-induction values were well predicted as shown in Fig. 3 (R^2 = 0.8058 and RMSE = 2.092 for CYP3A4, and R^2 = 0.9219 and RMSE = 0.890 for CYP2B6). In the regression models, lipophilicity is a main contributor to CYP3A4 induction and not only lipophilicity but also molecular polarity plays important roles for CYP2B6 induction.

Verification of the regression models.

To verify the regression models, induction assays with cryopreserved human hepatocytes were performed using another set of imidazole-containing compounds (validation compounds: Supplemental Figure 3). The physicochemical parameters of the validation compounds were obtained with QikProp and ChemBioDraw (Table 3, Supplemental Table 2) and the fold-induction values of the validation compounds were predicted using the established regression models for CYP3A4 and CYP2B6 induction. The predicted fold-induction values for both CYP3A4 and CYP2B6 were within 2-fold of the fold-inductions observed (Fig. 4, Table 4).

Applicability of the regression models.

To know the validity of the regression models for CYP3A4 and CYP2B6 induction, *in vitro* induction assays were performed using 23 marketed drugs, which were previously reported by

DMD Fast Forward. Published on May 20, 2016 as DOI: 10.1124/dmd.115.068619
This article has not been copyedited and formatted. The final version may differ from this version.

Fahmi et al. (2010) (Table 4). CYP3A4 induction by these drugs was predicted with the model, and the predicted values were within a 2-fold limit for 17 of the marketed drugs (73.9%) (Fig. 5, Table 4). Because various cut-off criteria were reported to define the inducers versus non-inducers with *in vitro* induction assays, the accuracy of the prediction for CYP3A4 induction with the models was evaluated using two cut-off categories: 1) a fold-induction of *CYP3A4* mRNA levels (2- and 4-fold) and 2) a fold-induction achieving 10% and 20% that for rifampicin (10 μM) (Table 5). The best concordance was achieved when "10% of rifampicin" was used as a cut-off criterion. Unlike CYP3A4 induction, CYP2B6 induction by these marketed drugs was not well predicted with the established models and in most cases the fold-induction was over-estimated (Fig. 5, Table 4, Supplemental Table 3).

Finally, the applicability of the CYP3A4 and CYP2B6 regression models in different lots of hepatocytes were investigated. CYP3A4 and CYP2B6 induction by the 22 test azole compounds were predicted with the models while the induction of CYP3A4 and CYP2B6 by these azole compounds was assessed in another lot of hepatocytes. The predicted values of CYP3A4 and CYP2B6 induction were within a 2-fold limit for 18 (81.8%) and 19 compounds (86.4%), respectively (Fig. 6).

DMD Fast Forward. Published on May 20, 2016 as DOI: 10.1124/dmd.115.068619
This article has not been copyedited and formatted. The final version may differ from this version.

Discussion

In this study we established the regression models for CYP3A4 and CYP2B6 inductions in human hepatocytes using physicochemical parameters calculated by commonly used software. As shown in Fig. 3, the predicted fold-induction values were strongly correlated with the observed values for both CYP3A4 and CYP2B6 when the multiple regression modeling was conducted using the compounds selected by PCA. Although the test compounds used in this study were congeneric compounds, the regression model for CYP3A4 induction could be applicable to structurally diverse compounds.

Since CYP induction was observed in cultured primary human hepatocytes and various methods have been reported to predict the clinical CYP3A4 induction from *in vitro* studies (Fahmi et al., 2008, 2009, and Kaneko et al., 2009), CYP induction assays using human hepatocytes and/or immortalized cell lines are usually performed in drug discovery and/or development processes to estimate the induction risk of new drug candidates (Fahmi et al., 2010). In addition, the evaluation in human hepatocytes is recognized as the most accepted approach by regulatory authorities, such as the U.S. Food and Drug Administration. However, because of the physicochemical properties (e.g., insufficient solubility) and/or cytotoxicity of test compounds, it is difficult to assess CYP induction for all of the compounds using human hepatocytes in early drug discovery and lead optimizing stages. Therefore, the prediction of CYP induction using in silico models is useful and desirable to evaluate the DDI risks of such compounds as well as those with synthetic difficulties, such as metabolites. Because the prediction models established in this study for CYP induction consist of only a few physicochemical parameters calculated with commercially available software, our models enable us to determine the potent inducers within a large number of compounds.

The multiple regression models first obtained using all of the azole compounds were unable to sufficiently predict CYP3A4 and CYP2B6 induction. Many ligands that activate

DMD Fast Forward. Published on May 20, 2016 as DOI: 10.1124/dmd.115.068619
This article has not been copyedited and formatted. The final version may differ from this version.

PXR can also activate CAR and there is overlap in the target genes of these two receptors (Maglich et al., 2002, 2003). In addition, the test azole compounds showed different abilities for inducing several CYPs, suggesting that these azole compounds might induce CYP enzymes through multiple mechanisms. Therefore, we selected the test azole compounds to establish good prediction models for CYP induction using PCA, which is commonly used to characterize and categorize data sets. The PCA results suggested that PC1 might represent the potency of CYP3A4 induction, PC2 might show the selectivity for CYP1A2 induction, and PC3 might be the selectivity for CYP2B6 induction. Based on these, predominant CYP3A4 inducers and potent CYP2B6 inducers were selected for modeling. This process greatly improved the accuracy of the regression models for both CYP3A4 and CYP2B6 induction; the adjusted coefficients of determination (R^2) were 0.8 and 0.9, respectively.

The variability in the CYP induction among different batches of hepatocytes is normally great. However our regression models showed that more than 80% of compounds could be predicted within 2-fold limited errors both CYP3A4 and CYP2B6 induction in different lots of cryopreserved primary hepatocytes after normalization with the fold-induction values of positive control compounds. Therefore, our regression models might be generally used to predict the potency of CYP induction even independently of hepatocytes lots.

Our final regression model for CYP3A4 induction contains lipophilicity as the main determinant. In fact, the validation compounds **E**, **F**, and **G** have low clogP values compared with compound **D**, and the predicted and observed fold-induction values of **E**, **F**, and **G** were lower than compound **D**. Conversely, compounds **H**, **I**, **J**, **K**, and **L**, which have high clogP values compared to compound **D**, showed higher fold-induction values than compound **D**. Similar results were obtained for non-azole compounds; pleconaril, a known CYP3A4 inducer, clearly increased *CYP3A4* mRNA levels. Several marketed drugs including aprepitant, avasimive, bosentan, efavirenz, terbinafine, and torglitazole, having high clogP values and

DMD Fast Forward. Published on May 20, 2016 as DOI: 10.1124/dmd.115.068619
This article has not been copyedited and formatted. The final version may differ from this version.

increased the *CYP3A4* mRNA levels much more than pleconaril did. A chlorine atom is often used to increase the lipophilicity and molecular size in the lead-optimizing process. Econazole has a similar structure to isoconazole and miconazole but contains fewer chlorine atoms, suggesting that CYP3A4 induction by econazole is weaker than those by isoconazole and miconazole. The results of the induction assays demonstrated that this prediction was correct. Considering the induction mechanism, Yoshida et al. (2012) reported that PXR agonists tend to be more lipophilic and larger in molecular size than non-agonists. In addition, Ung et al. (2007) reported that PXR activators contain more halogen atoms, especially chlorine atoms, than non-activators. In summary, our regression model for CYP3A4 induction agrees with these reports, which demonstrates the reliability and applicability of our model.

In contrast to the prediction of CYP3A4 induction, our regression model for CYP2B6 induction seems to have structural limitations. For compounds containing imidazole and triazole moieties, the predicted CYP2B6 fold-induction values were within 2-fold of the observed values, whereas the predicted values of the marketed drugs, non-azole compounds, tended to be over-estimated. Currently, the majority of identified CYP3A4 and CYP2B6 inducers are known activators of PXR but not CAR (Faucette et al., 2004). Only a limited number of compounds, including CITCO and phenytoin, were shown to induce CYP3A4 and/or CYP2B6 preferentially through CAR (Maglich et al., 2003, Wang et al., 2004), with stronger induction of CYP2B6 than CYP3A4. For 52% of the marketed drugs used, the fold-induction ratio of CYP3A4/CYP2B6 was higher than that of phenobarbital (CYP3A4/CYP2B6: 1.37) (data not shown). Therefore, most of the marketed drugs used in this study might be preferential CYP3A4 inducers through PXR activation.

In addition, CAR is activated through two different mechanisms: 1) activation by direct binding of agonists, such as CITCO for human CAR (Maglich et al., 2003), and 2) indirect activation through phosphorylation/dephosphorylation signals (Sueyoshi and Negishi, 2001,

Mutoh et al., 2013). Phenobarbital, which is commonly used as a positive control for CYP2B6 induction, activates CAR through the latter mechanism (Mutoh et al., 2013). Generally, higher concentrations are needed to achieve significant CYP2B6 induction for these indirect activators compared with direct activators or ligands. Therefore, the reason for the poor applicability of the regression model for CYP2B6 induction might result from the use of fold-induction values at a fixed concentration of 10 μM in this study. In fact, when we used Emax values of CYP2B6 induction, the maximum fold-induction value observed in the concentration range used, instead of the fold-induction values at 10 μM as the observed values for the marketed drugs, the correlation between the predicted and observed values improved; the prediction of 14 compounds (60%) was within a 2-fold limit (data not shown). These results suggest that the marketed drugs used in this study need higher concentrations to achieve Emax compared with the azole-containing compounds. Thus, the regression model for CYP2B6 induction established by azole compounds probably has structural and/or mechanistic limitations.

Conazoles are widely used as antifungal drugs, although their potent abilities for CYP inhibition and induction limit their clinical application by systematic treatment. First-generation conazoles, such as miconazole, econazole, and isoconazole, are mainly used to treat superficial mycoses, and second/third-generation conazoles, such as fluconazole and voriconazole, are applied to treat emerging invasive fungal infections (Heeres et al., 2010). Because there is a need for more powerful and easy-to-use antifungal drugs for invasive infections, some conazoles, such as albaconazole, ravuconazole, isavuconazole, and pramiconazole, have been developed and/or marketed. Our regression model could aid in developing a conazole with an advantage in pharmacokinetics and DDIs showing no or less potency for CYP3A4 and CYP2B6 induction.

In conclusion, the quantitative regression models for CYP3A4 and CYP2B6 induction

were established with a few physicochemical parameters, even though there were limitations with the CYP2B6 induction model. Because CYP3A enzymes, including CYP3A4, account for 30% of the CYPs in human livers and mediate the metabolism of more than 60% of marketed drugs (di Masi et al., 2009), the CYP3A4-associated DDIs should be avoided at first. Our regression models for CYP induction provide a useful and promising method to obtain compounds with less DDI risk during the drug screening process without chemical synthesis.

Authorship Contributions

Participated in research design: Nagai, Konno, Satsukawa, Yamashita, and Yoshinari

Conducted experiments: Nagai and Yoshinari

Performed data analysis: Nagai and Yoshinari

Wrote or contributed to the writing of the manuscript: Nagai and Yoshinari

References

di Masi A, De Marinis E, Ascenzi P, and Marino M (2009) Nuclear receptors CAR and PXR: Molecular, functional, and biomedical aspects. *Mol Aspects Med* **30**:297–343

Dingemanse J and van Giersbergen PL (2004) Clinical pharmacology of bosentan, a dual endothelin receptor antagonist. *Clin Pharmacokinet* **43**:1089–1115

Dybdahi M, Nikolov NG, Wedebye EB, Jónsdóttir SÓ, and Niemalä JR (2012) QSAR model for human pregnane X receptor (PXR) binding: screening of environmental chemicals and correlations with genotoxicity, endocrine disruption and teratogenicity. *Toxicol Appl Pharmacol* **262**: 301–309

Fahmi OA, Boldt S, Kish M, Obach RS, and Tremaine LM (2008) Prediction of drug-drug interactions from in vitro induction data: application of the relative induction score approach using cryopreserved human hepatocytes. *Drug Metab Dispos* **36**:1971–1974

Fahmi OA, Hurst S, Plowchalk D, Cook J, Guo F, Youdim K, Dickins M, Phipps A, Darekar A, Hyland R, and Obach RS (2009) Comparison of different algorithms for predicting clinical drug-drug interactions, based on the use of CYP3A4 in vitro data: predictions of compounds as precipitants of interactions. *Drug Metab Dispos* **37**:1658–1666

Fahmi OA, Kish M, Boldt S, and Obach RS (2010) Cytochrome P450 3A4 mRNA is a more reliable marker than CYP3A4 activity for detecting pregnane X receptor-activated induction of drug-metabolizing enzymes. *Drug Metab Dispos* **38**:1605–1611

Faucette SR, Wang H, Hamilton GA, Jolley SL, Gilbert D, Lindley C, Yan B, Negishi M, and LeCluyse EL (2004) Regulation of CYP2B6 in primary human hepatocytes by prototypical inducers. *Drug Metab Dispos* **32**:348–358

Goetz AK, Bao W, Ren H, Schmid JE, Tully DB, Wood C, Rockett JC, Narotsky MG, Sun G, Lambert GR, Thai SF, Wolf DC, Nesnow S, and Dix DJ (2006) Gene expression profiling in the liver of CD-1 mice to characterize the hepatotoxicity of triazole fungicides. *Toxicol*

Appl Pharmacol **215**:278–284

Handa K, Nagamome I, Yamaotsu N, Gouda H, and Hirono S (2015) Three-dimensional quantitative structure-activity relationship analysis for human pregnane X Receptor fot the prediction of CYP3A4 induction in human hepatocytes: structure-based domparative molecular field analysis. *J Pharm Sci* **104**: 223–232

Heeres J, Meerpoel L, and Lewi P (2010) Conazoles. *Molecules* **15**:4129–4188

Imai J, Yamazoe Y, and Yoshinari K (2013) Novel cell-based reporter assay system using epitope-tagged protein for the identification of agonistic ligands of constitutive androstane receptor (CAR). *Drug Metab Pharmacokinet* **28**: 290–298

Juberg DR, Mudra DR, Hazelton GA, and Parkinson A (2006) The effect of fenbuconazole on cell proliferation and enzyme induction in the liver of female CD1 mice. *Toxicol Appl Pharmacol* **214**:178–187

Kaneko A, Kato M, Sekiguchi N, Mitsui T, Takeda K, and Aso Y (2009) *In vitro* model for the prediction of clinical CYP3A4 induction using HepaRG cells. Xenobiotica **39**:803–810

Khandelwal A, Krasowski MD, Reschly EJ, Sinz MW, Swaan PW, and Ekins S (2008) Machine learning methods and docking for predicting human pregnane X receptor activation. *Chem Res Toxicol* **21**: 14571467

LeCluyse EL (2001) Pregnane X receptor: molecular basis for species differences in CYP3A induction by xenobiotics. *Chem Biol Interact* **134**: 283–289

Luo G, Cunningham M, Kim S, Burn T, Lin J, Sinz M, Hamilton G, Rizzo C, Jolley S, Gilvert D, Downey A, Mudra D, Graham R, Carroll K, Xie J, Madan A, Parkinson A, Christ D, Selling B, LeCluyse E, and Gan LS (2002) CYP3A4 induction by drugs: correlation between a pregnane X receptor reporter gene assay and CYP3A4 expression in human hepatocytes. *Drug Metab Dispos* **30**:795–804

Maglich JM, Stoltz CM, Goodwin B, Hawkins-Brown D, Moore JT, and Kliewer SA (2002)

Nuclear pregnane X receptor and constitutive androstane receptor regulate overlapping but distinct sets of genes involved in xenobiotic detoxification. *Mol Pharmacol* **62**:638–646

Maglich JM, Parks DJ, Moore LB, Collins JL, Goodwin B, Billin AN, Stoltz CA, Kliewer SA, Lambert MH, Willson TM, and Moore JT (2003) Identification of a novel human constitutive androstane receptor (CAR) agonist and its use in the identification of CAR target genes. *J Biol Chem* **278**:17277–17283

Matsuura Y, Kotani E, Ito T, Fukuda T, Tobinaga S, Yoshida T, and Kuroiwa Y (1991) Structure-activity relationships in the induction of hepatic microsomal cytochrome P450 by clotrimazole and its structurally related compounds in rats. *Biochem Pharmacol* **41**:1949–1956

Mishra NK, Agarwal S, and Raghava GP (2010) Prediction of cytochrome P450 isoform responsible for metabolizing a drug molecule. *BMC Pharmacol* **10**:8–16

Mutoh S, Sobhany M, Moore R, Perera L, Pedersen L, Sueyoshi T, and Negishi M (2013) Phenobarbital indirectly activates the constitutive active androstane receptor (CAR) by inhibition of epidermal growth factor receptor signaling. *Sci Signal* **6**: ra31

Niemi M, Backman JT, Fromm MF, Neuvonen PJ, and Kivistö KT (2003) Pharmacokinetic Interactions with rifampicin : clinical relevance. *Clin Pharmacokinet* **42**:819–850

Niwa T, Imagawa Y, and Yamazaki H (2014) Drug interactions between nine antifungal agents and drugs metabolized by human cytochromes P450. *Curr Duf Metab* **15**:651–79

Ohbuchi M, Yoshinari K, Kaneko H, Matsumoto S, Inoue A, Kawamura A, Usui T, and Yamazoe Y (2013) Coordinated roles of pregnane X receptor and constitutive androstane receptor in autoinduction on voriconazole metabolism in mice. *Antimicrob Agents Chemother* **57**:1332–1338

Sahi J, Milad MA, Zheng X, Rose KA, Wang H, Stilgenbauer L, Gilbert D, Jolley S, Stern

RH, and LeCluyse EL (2003) Avasimibe induces CYP3A4 and multiple drug resistance protein 1 gene expression through activation of the pregnane X receptor. *J Pharmacol Exp Ther* **306**:1027–1034

Sahi J, Shord SS, Lindley C, Ferguson S, and LeCluyse EL (2009) Regulation of cytochrome P450 2C9 expression in primary cultures of human hepatocytes. *J Biochem Mol Toxicol* **23**:43–58

Sueyoshi T and Negishi M (2001) Phenobarbital response elements of cytochrome P450 genes and nuclear receptors. *Annu Rev Pharmacol Toxicol* **41**: 123–143

Sun G, Tahi SF, Lambert GR, Wolf DC, Tully DB, Goetz AK, George MH, Grindstaff RD, Dix DJ, and Nesnow S (2006) Fluconazole-induced hepatic cytochrome P450 gene expression and enzymatic activities in rats and mice. *Toxicol Lett* **164**:44–53

Sun G, Grindstaff RD Thai SF, Lambert GR, Tully DB, Dix DJ, and Nesnow S (2007) Induction of cytochrome P450 enzymes in rat liver by two conazoles, myclobutanil and triadimefon. *Xenobiotica* **37**:180–193

Tamura K, Inoue K, Takahashi M, Matsuo S, Irie K, Kodama Y, Ozawa S, Nishikawa A, and Yoshida M (2013) Dose-response involvement of constitutive androstane receptor in mouse liver hypertrophy induced by triazole fungicides. *Toxicol Lett* **221**:47–56

Ung CY, Li H, Yap CW, and Chen YZ (2007) In silico prediction of pregnane X receptor activators by machine learning approaches. *Mol Pharmacol* **71**:158–168

Wanchana S, Yamashita F, and Hashida M (2003) QSAR analysis of the inhibition of recombinant CYP 3A4 activity by structurally diverse compounds using a genetic algorithm-combined partial least squares method. *Pharm Res* **20**:1401–1408

Wang H, Faucette S, Moore R, Sueyoshi T, Negishi M, and LeCluyse E (2004) Human constitutive androstane receptor mediates induction of CYP2B6 gene expression by phenytoin. *J Biol Chem* **279**:29295–29301

Wei P, Zhang J, Dowhan DH, Han Y, and Moore DD (2002) Specific and overlapping functions of the nuclear hormone receptors CAR and PCR in xenobiotic response. *Pharmacogenomics J* **2**:117–126

Wu B, Li S, and Dong D (2013) 3D structures and ligand specificities of nuclear xenobiotic receptors CAR, PXR and VDR. *Drug Discov Today* **18**: 574–581

Xiao L, Nickbarg E, Wang W, Thomas A, Ziebell M, Prosise WW, Lexburg CA, Taremi SS, Gerlach VL, Le HV, and Cheng KC (2011) Evaluation of in vitro PXR-based assays and in silico modeling approaches for understanding the binding of a structurally diverse set of drugs to PXR. *Biochem Pharmacol* **81**: 669–679

Yoshida S, Yamashita F, Itoh T, and Hashida M (2012) Structure-activity relationship modeling for predicting interactions with pregnane X receptor by recursive partitioning. *Drug Metab Pharmacokinet* **27**:506–512

Figure Legends

Fig. 1. Chemical structures of the test azole compounds.

Fig. 2. Loading and score plots of the test azole compounds from PCA. A, loading plots of PC1 vs. PC2. B, loading plots of PC1 vs. PC3. C, score plots of PC1 vs. PC2. D, score plots of PC1 vs. PC3. Compounds in shadow areas were considered preferential CYP3A4 inducers (C) and potential CYP2B6 inducers (D).

Fig. 3. Correlation of the predicted and observed fold-induction values of CYP3A4 (A) and CYP2B6 (B) induction by selected compounds. Correlation analyses were performed on the compounds selected by PCA in Fig. 2. The solid line in each graph is the line of unity and the dotted lines indicate a 2-fold limit. The observed fold-induction is shown as the mean ± S.D. (n = 3 to 6, “n” means the number of wells in a single hepatocyte experiment).

Fig. 4. Correlation between the predicted and observed fold-induction values of CYP3A4 (A) and CYP2B6 (B) induction for the azole-containing validation compounds. The solid line in each graph is the line of unity and the dotted lines indicate a 2-fold limit. The observed fold-induction is shown as the mean ± S.D. (n = 3, “n” means the number of wells in a single hepatocyte experiment).

Fig. 5. Correlation between the predicted and observed fold-induction values of CYP3A4 (A) and CYP2B6 (B) induction for the marketed drugs. The solid line in each graph is the line of unity and the dotted lines indicate a 2-fold limit. When the predicted fold-induction values were under 1, they were plotted at 1. The observed fold-induction values from one experiment are shown.

Fig. 6. Correlation between the predicted and observed fold-induction values of CYP3A4 (A) and CYP2B6 (B) induction for the test azole compounds in a different lot of cryopreserved human hepatocytes. The solid line in each graph is the line of unity and the dotted lines indicate a 2-fold limit. When the predicted fold-induction values were under 1, they were plotted at 1. The observed fold-induction is shown as the mean ± S.D. (n = 3 to 6, “n” means the number of wells in a single hepatocyte experiment).

TABLE 1 Fold-induction of CYP1A2, CYP2B6, CYP2C9, and CYP3A4 for test azole and reference compounds.

Compounds	Fold-induction				Ratio
	CYP1A2	CYP2B6	CYP2C9	CYP3A4	(3A4/2B6)
Azoles					
Bifonazole	11.35	5.42	1.12	6.89	1.27
Climbazole	4.08	6.79	1.65	12.13	1.79
Clotrimazole	4.44	8.26	1.84	17.05	2.06
Econazole	8.11	6.44	1.35	5.45	0.85
Fenbuconazole	3.14	7.36	1.96	7.42	1.01
Fluconazole	0.97	1.57	1.20	1.59	1.01
Hexaconazole	3.21	6.25	1.85	6.76	1.08
Imazalil	6.31	9.04	1.66	9.81	1.09
Isoconazole	3.30	8.45	2.14	11.99	1.42
Lanoconazole	7.91	12.35	1.13	7.62	0.62
Luliconazole	9.32	9.20	1.37	5.23	0.57
Miconazole	6.41	7.52	1.74	13.90	1.85
Metabolite of miconazole	1.40	3.82	1.02	2.89	0.76
Myclobutanil	1.90	8.06	1.72	6.96	0.86
Oxiconazole	9.29	6.34	1.27	8.12	1.28
Propiconazole	3.74	7.00	2.05	6.83	0.98
Tebuconazole	3.49	5.29	1.69	5.99	1.13
Tioconazole	3.12	7.75	1.34	4.45	0.57
Trihlumizole	3.38	5.62	1.20	5.84	1.04
Uniconazole	5.52	11.22	2.00	8.33	0.74
Voriconazole	1.27	2.72	1.26	3.60	1.32
Metabolite of voriconazole	1.04	1.42	0.92	1.06	0.75
Reference compounds					
Rifampicin (10 μM)	0.87	9.78	2.79	32.20	3.29
Phenobarbital (750 μM)	1.40	15.78	2.83	21.56	1.37
3-MC (1 μM)	16.40	2.14	1.29	0.72	0.34
CITCO (1 μM)	0.92	7.43	1.07	3.43	0.46
Probenecid (10 μM)	1.10	1.71	1.28	1.89	1.11

Each fold-induction value represents the mean (n = 3 to 6, “n” means the number of wells in a single hepatocyte experiment)

TABLE 2 Physicochemical parameters of the test azole compounds.

Compounds	clogP	PISA	WPSA	EA	SA fluorine
Bifonazole	4.991	576.9	0.00	0.670	0.00
Climbazole	3.426	222.6	71.70	0.360	0.00
Clotrimazole	5.254	511.5	36.47	0.459	0.00
Econazole	5.099	343.9	198.42	0.766	0.00
Fenbuconazole	3.557	354.9	71.64	0.278	0.00
Fluconazole	-0.440	262.5	80.56	1.028	80.56
Hexaconazole	3.556	185.7	116.34	0.623	0.00
Imazalil	3.646	268.2	108.88	0.705	0.00
Isoconazole	5.812	346.2	183.11	0.674	0.00
Lanoconazole	2.780	292.2	112.35	1.487	0.00
Luliconazole	3.493	245.2	184.00	1.528	0.00
Miconazole	5.812	309.1	257.69	0.774	0.00
Metabolite of miconazole	2.160	242.7	121.46	0.641	0.00
Myclobutanil	3.197	199.5	71.68	0.692	0.00
Oxiconazole	6.800	316.1	253.26	0.703	0.00
Propiconazole	3.532	173.0	107.13	0.452	0.00
Tebuconazole	3.260	203.3	71.64	-0.032	0.00
Tioconazole	4.787	300.6	203.37	0.721	0.00
Triflumizole	4.047	203.2	156.15	0.969	88.26
Uniconazole	3.610	163.0	107.23	0.977	0.00
Voriconazole	0.523	278.4	98.46	1.287	98.46
Metabolite of voriconazole	0.430	229.1	76.98	0.753	76.98

clogP; calculated logP, PISA; π (carbon and attached hydrogen) component of the total solvent accessible surface area (SASA), WPSA; weakly

polar component of the SASA (halogens, P, and S), EA; calculated electron affinity, and SA Fluorine; solvent-accessible surface area of fluorine atoms

TABLE 3 Physicochemical parameters and predicted and observed fold-induction values of azole-containing validation compounds.

Compounds	clogP	PISA	WPSA	EA	SA fluorine	CYP3A4 induction		CYP2B6 induction	
						Observed	Predicted	Observed	Predicted
A	3.708	436.2	48.67	0.766	0.00	10.38	11.50	12.58	11.71
B	3.785	253.4	42.46	0.615	0.00	8.93	8.35	7.15	11.22
C	2.746	243.3	51.78	0.747	0.00	6.07	6.30	10.65	9.58
D	2.273	255.9	46.44	0.628	0.00	8.09	5.68	14.51	8.17
E	2.059	249.6	0.00	0.500	0.00	6.44	5.19	11.66	9.11
F	1.479	240.1	0.00	0.390	0.00	3.94	3.98	6.99	7.30
G	0.893	248.4	0.00	0.559	0.00	3.52	3.07	9.66	7.20
H	3.247	370.2	0.00	0.352	0.00	17.03	9.49	12.81	10.51
I	3.390	401.9	23.05	0.422	23.05	15.68	10.31	12.06	9.38
J	3.390	340.8	35.87	0.413	35.87	14.70	9.21	12.62	8.31
K	3.390	332.9	47.02	0.426	47.02	10.49	9.07	9.68	7.50
L	3.533	317.4	58.76	0.651	58.76	12.81	9.05	10.26	8.22

Each fold-induction value represents the mean (n = 3, “n” means the number of wells in a single hepatocyte experiment).

The abbreviations for the physicochemical parameters are shown in Table 2.

TABLE 4 Physicochemical parameters and predicted and observed fold-induction values of marketed drugs.

Drugs	clogP	PISA	WPSA	EA	SA fluorine	CYP3A4 induction		CYP2B6 induction	
						Observed	Predicted	Observed	Predicted
Aprepitant	4.600	152.4	262.69	1.025	262.69	15.40	7.99	0.89	1.00
Avasimibe	9.700	106.5	0.00	1.182	0.00	19.26	16.34	5.57	27.91
Bosentan	4.170	339.1	0.29	1.171	0.00	12.67	10.58	5.39	17.23
Carbamazepine	2.380	325.5	0.00	0.709	0.00	5.54	7.11	4.69	10.94
Efavirenz	4.670	110.6	165.31	0.785	95.15	11.80	7.37	9.61	5.07
Ethinyl estradiol	0.830	151.3	0.00	-0.285	0.00	7.14	1.19	6.06	1.78
Flumazenil	1.290	161.0	46.92	1.395	46.92	1.22	2.19	1.67	9.38
Fluoxetine	4.570	293.7	116.79	0.302	116.79	4.55	10.48	1.02	3.29
Fulvoxamine	3.320	128.9	116.80	0.736	116.80	4.57	5.27	2.91	3.59
Gatifloxacin	-0.260	57.4	33.31	1.278	33.31	1.08	1.00	1.28	6.76
Leflunomide	2.320	189.1	116.83	0.829	116.83	1.58	4.55	4.28	2.25
Nafcillin	3.530	195.6	29.61	0.965	0.00	3.97	6.85	1.40	13.41
Nevirapine	2.650	224.4	0.00	0.741	0.00	1.56	5.78	2.83	11.65
Nifedipine	3.120	136.4	0.00	0.553	0.00	9.09	5.04	5.62	11.38
Phenobarbital	1.370	170.1	0.00	0.550	0.00	1.48	2.50	1.52	8.01
Phenytoin	2.090	340.5	0.00	0.283	0.00	5.85	6.86	7.71	7.73
Pioglitazone	3.530	236.7	32.30	0.875	0.00	10.64	7.58	3.30	12.73
Pleconaril	4.040	130.2	128.15	1.578	128.15	5.17	6.59	5.82	9.31
Ranitidine	0.670	88.3	27.97	0.364	0.00	1.04	1.00	1.77	4.26
Rosigilitazone	3.020	297.4	32.26	0.867	0.00	4.81	7.76	1.26	11.70
Terbinafine	5.960	296.0	0.00	0.656	0.00	12.34	13.02	5.27	17.47
Topiramate	0.040	0.0	0.31	0.651	0.00	2.55	1.00	1.79	6.08
Troglitazone	5.590	153.4	32.30	0.896	0.00	19.85	9.79	7.90	16.81

When the predicted fold-induction values were under 1, they were represented as 1. Each observed fold-induction value from one experiment is shown.

The abbreviations for the physicochemical parameters are shown in Table 2.

TABLE 5 Summary of the prediction for CYP3A4 induction using marketed drugs.

Cut-off criteria	Number of drugs				Sensitivity (%)	Specificity (%)	Concordance (%)
	True Positive	False Positive	True Negative	False Negative			
2-fold	15	4	2	2	88.2	33.3	73.9
4-fold	14	3	5	1	93.3	62.5	82.6
10% of rifampicin	15	2	5	1	93.8	71.4	87.0
20% of rifampicin	7	6	8	2	77.8	57.1	65.2

Figure 1

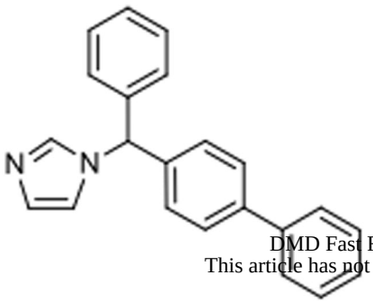

Bifonazole

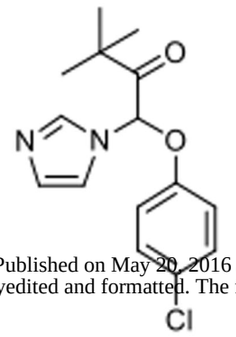

Climbazole

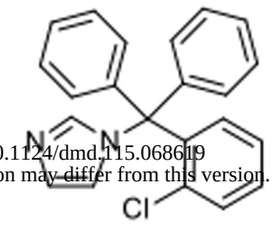

Climbazole

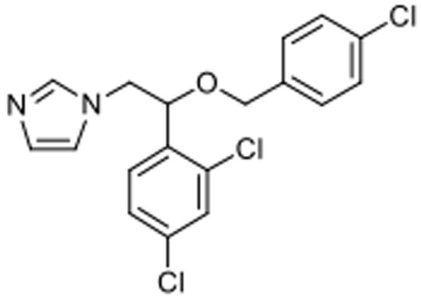

Econazole

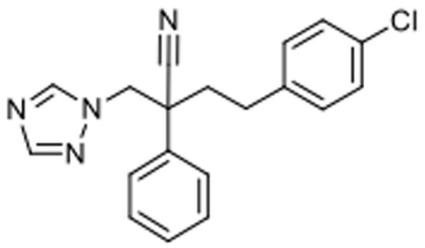

Fenbuconazole

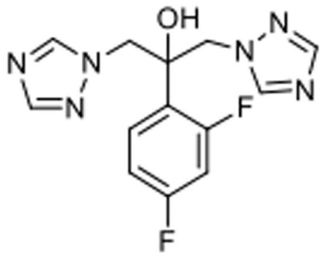

Fluconazole

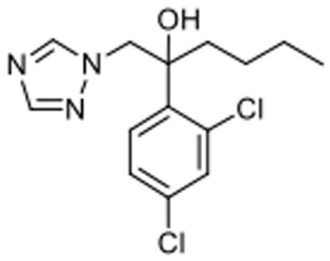

Hexaconazole

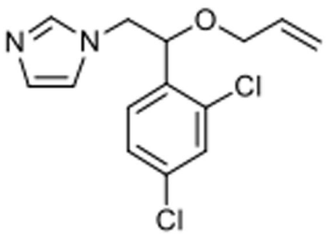

Imazalil

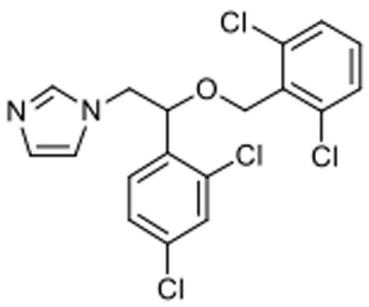

Isoconazole

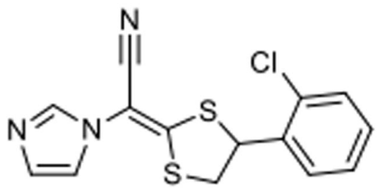

Lanoconazole

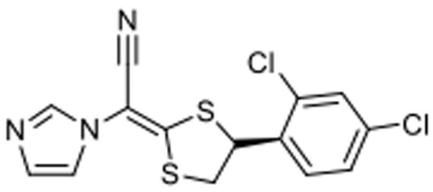

Luliconazole

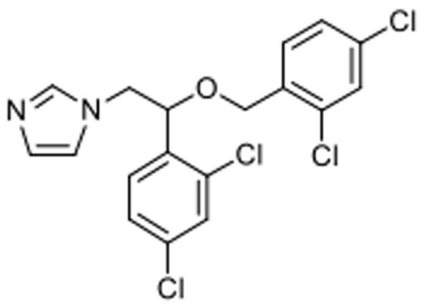

Miconazole

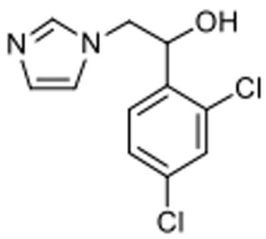

Metabolite of miconazole

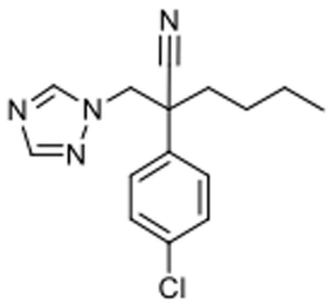

Myclobutanil

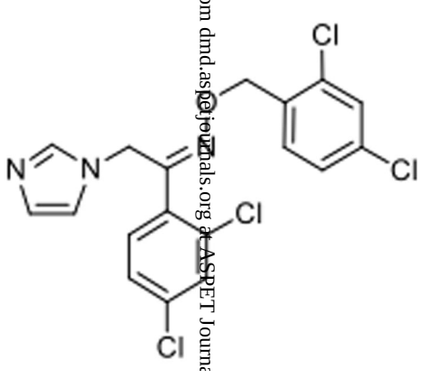

Oxiconazole

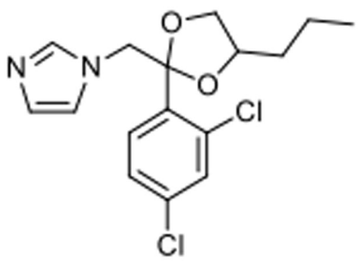

Propiconazole

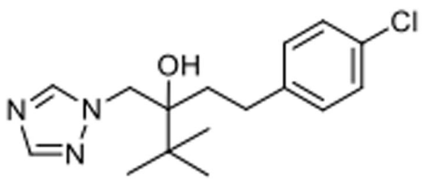

Tebuconazole

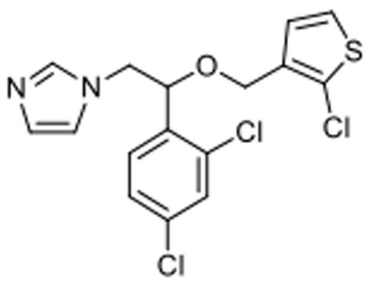

Tioconazole

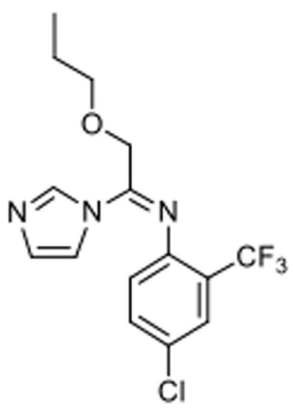

Triflumizole

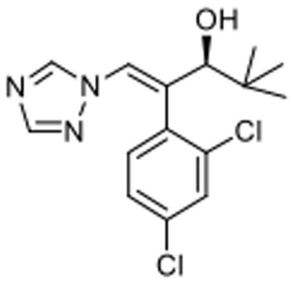

Uniconazole

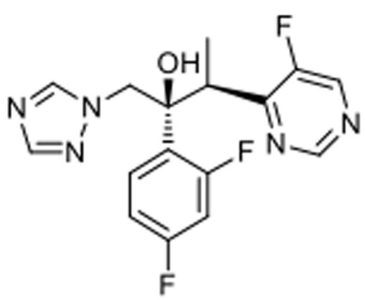

Voriconazole

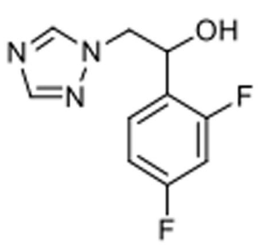

Metabolite of voriconazole

Figure 2

DMD Fast Forward. Published on May 20, 2016 as DOI: 10.1124/dmd.115.068619
This article has not been copyedited and formatted. The final version may differ from this version.

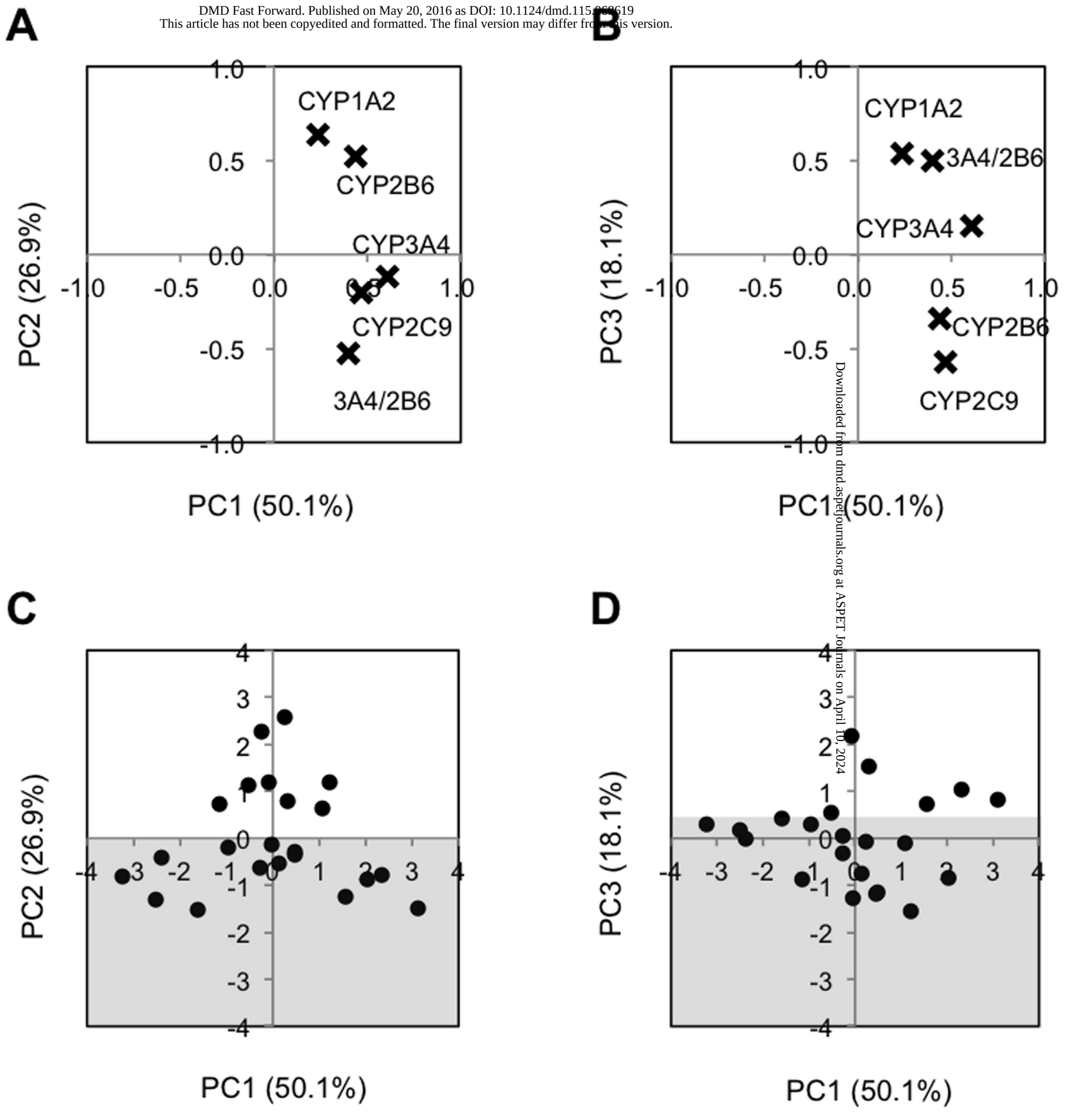

Figure 3

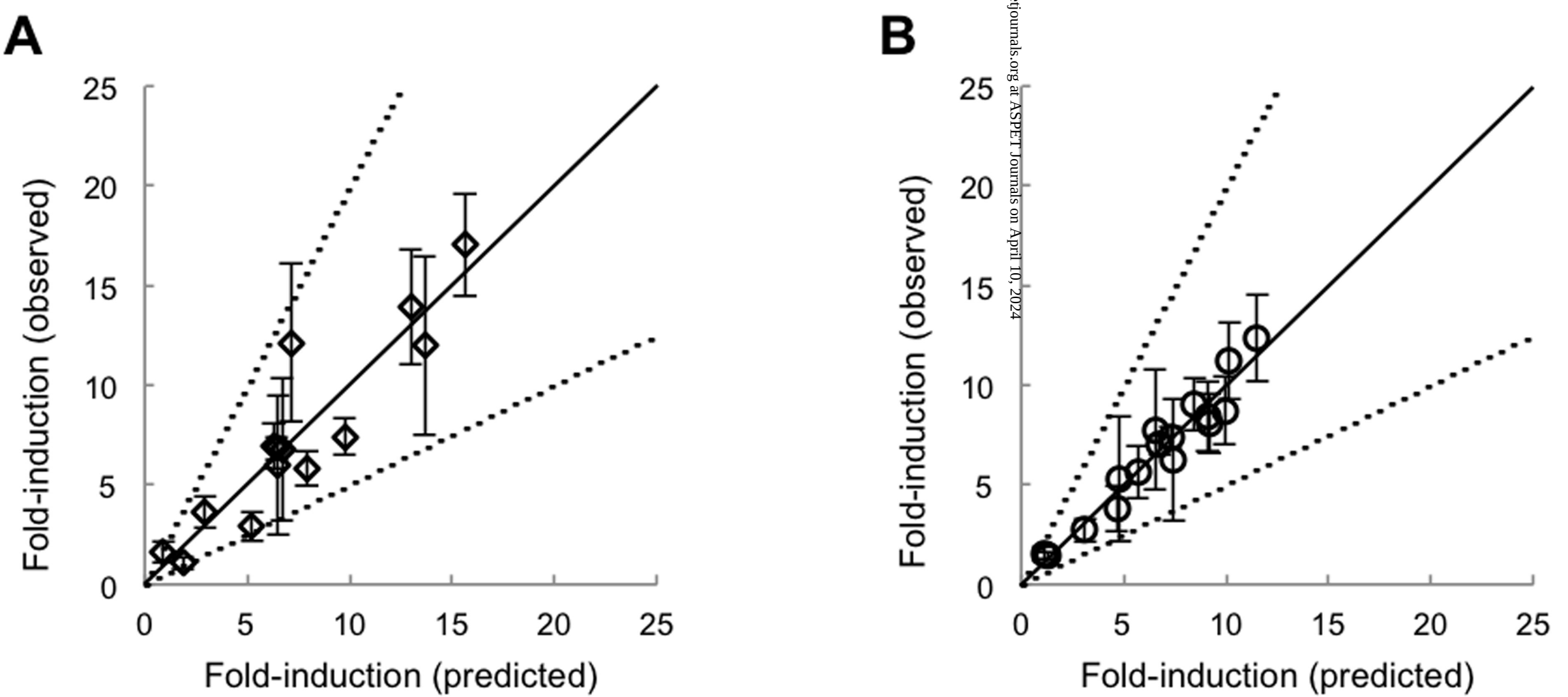

Figure 4

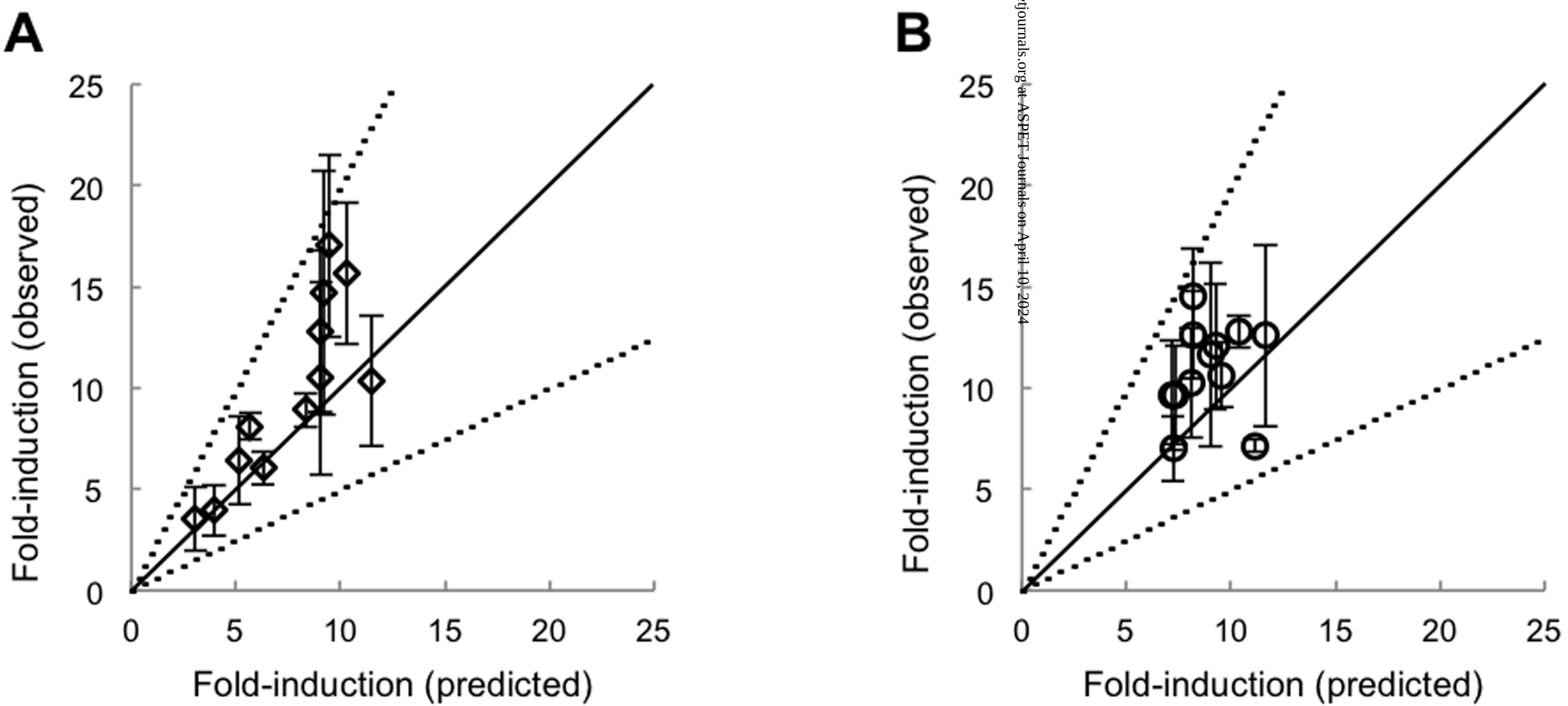

Figure 5

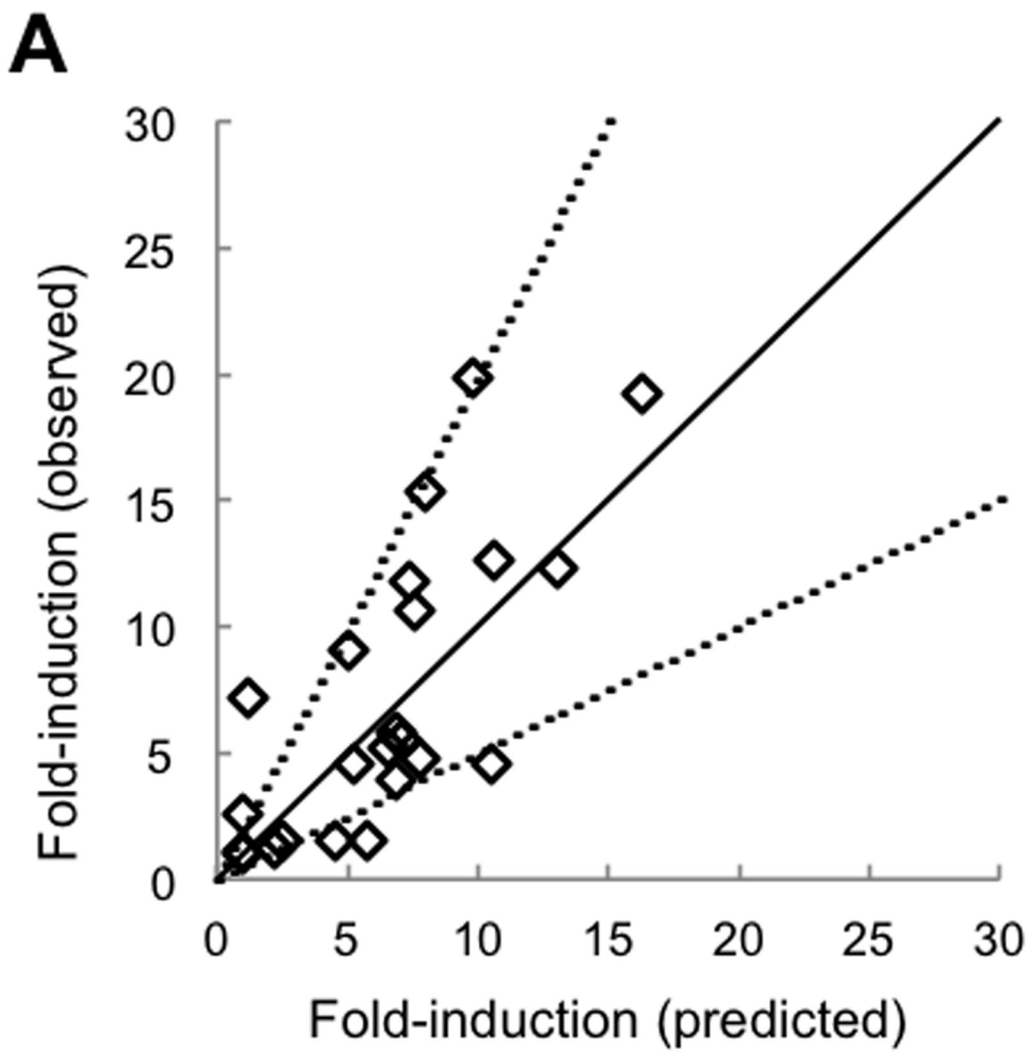

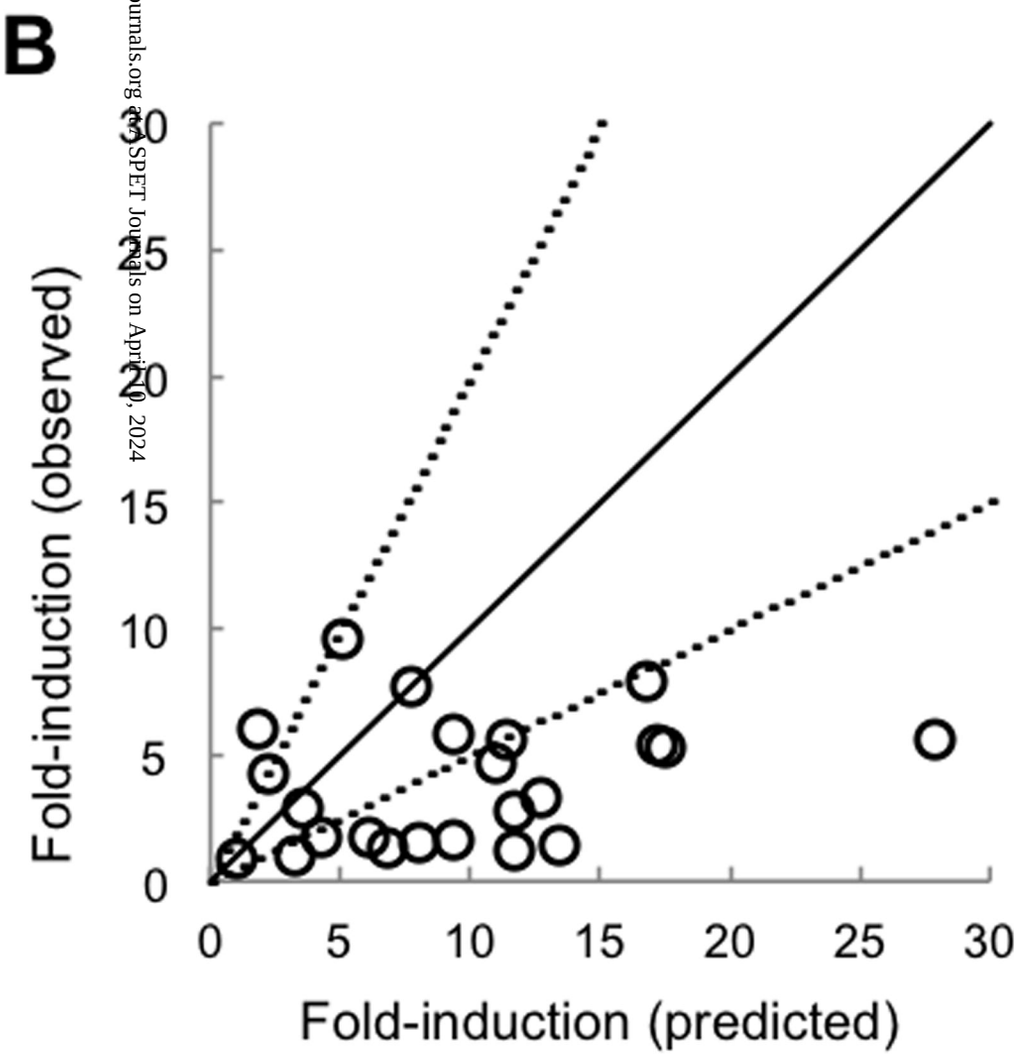

Figure 6